

Elastic properties of few unit cell thick superconducting crystals of $\text{Bi}_2\text{Sr}_2\text{CaCu}_2\text{O}_{8+\delta}$

Sudhir Kumar Sahu,¹ Digambar Jangade,² Arumugam Thamizhavel,² Mandar M. Deshmukh,² and Vibhor Singh^{1, a)}

¹⁾Department of Physics, Indian Institute of Science, Bangalore-560012 (India)

²⁾Department of condensed matter physics and material sciences, Tata Institute of Fundamental Research, Mumbai - 400005 (India)

(Dated: 6 March 2024)

We present systematic measurements of the mechanical properties of few unit cell (UC) thick exfoliated crystals of a high- T_c cuprate superconductor $\text{Bi}_2\text{Sr}_2\text{CaCu}_2\text{O}_{8+\delta}$. We determine the elastic properties of these crystals by deformation using an atomic force microscope (AFM) at room temperature. With the spatial measurements of local compliance and their detailed modeling, we independently determine the Young's modulus of rigidity and the pre-stress. The Young's modulus of rigidity is found to be in the range of 22 GPa to 30 GPa for flakes with thickness from ~ 5 UC to 18 UC. The pre-stress spreads over the range of 5 MPa - 46 MPa, indicating a run-to-run variation during the exfoliation process. The determination of Young's modulus of rigidity for thin flakes is further verified from recently reported buckling technique.

There has been a keen interest towards the use of two-dimensional (2D) thin materials for device applications. While the electrical properties of these materials cover a wide spectrum ranging from insulating, semiconducting, metallic to superconducting behavior, their mechanical properties such as modulus of rigidity, fracture-strain, and thermal expansion are equally intriguing^{1,2}. This remarkable combination of characteristics make these materials accessible to novel applications such as flexible electronics and hybrid nanoelectromechanical systems for sensing applications³⁻⁶.

For nanoelectromechanical devices, materials with high electrical conductivity, and low mass are often preferred, as these properties tend to minimize the losses and improve the displacement transduction³⁻⁶. The mechanical properties of few unit cells (UC) thick exfoliated crystals could be significantly different from its bulk counterpart, resulting in interesting effects such as nonlinear damping⁷, and Duffing phenomena⁸. In addition, measurements of the elastic response could be a sensitive probe to the electronic or structural phase transitions in these materials⁹. This has led to a considerable investigation into the nanomechanical properties of materials such as graphene, MoS_2 , NbSe_2 , etc.¹⁰⁻¹⁵.

Recently, few UC thick crystals of high-transition temperature superconductor $\text{Bi}_2\text{Sr}_2\text{CaCu}_2\text{O}_{8+\delta}$ (BSCCO) have attracted attention due to their unique superconducting phase diagram, and applications towards cavity-optomechanical devices^{6,16-18}. While the elastic coefficients of the bulk crystals of BSCCO have been observed with large variations, there is no investigation into the elastic properties of few UC thick nanoscale samples^{19,20}. Here we report the measurement of Young's modulus of rigidity (E) and pre-stress (σ) on few UC thick superconducting crystals of BSCCO. These properties are helpful in engineering the resonant frequency of mechanical resonators for composite devices. In addition, determination of the Young's modulus of rigidity by two different

methods, on the crystals grown in the same run, brings clarity to the previously reported results from bulk-crystals^{19,20}.

We have primarily used elastic deformation by an AFM tip to measure the Young's modulus of rigidity and the pre-stress in exfoliated flakes of BSCCO. In total, we have studied 7 mesoscopic samples having thickness in the range of 16 nm to 55 nm, corresponding to ~ 5 UC to 18 UC thick crystals. We have performed measurements of the local compliance of the suspended flakes of BSCCO. Detailed finite-element modeling is then carried out to extract the Young's modulus and the pre-stress from compliance measurements. In addition, we employ a recently reported buckling technique to independently measure the Young's modulus for thin flakes²¹. We find that the results from the buckling technique are consistent with the AFM technique.

High-quality single-crystals of BSCCO were prepared by annealing melt-quenched shards in oxygen atmosphere. The BSCCO shards were prepared by heating the BSCCO powder (Sigma Aldrich - 365106) in a high-quality recrystallized alumina crucible. After the annealing step, these crystals are stored in liquid nitrogen and are only taken out at the time of mechanical exfoliation²². To prepare the samples for AFM measurements, we first use photolithography to pattern circular trenches in photoresist (S1813) on a 285 nm thick SiO_2 coated silicon substrate. It is followed by a step of reactive-ion etching of SiO_2 using a low-pressure fluorine plasma. This results in circular trenches having diameter from 1.8 to 6 μm on the substrate. Thin flakes of BSCCO are exfoliated by a scotch tape and transferred on top of the patterned substrate using a polydimethylsiloxane (PDMS) based dry exfoliation technique²³.

Fig. 1 (a) shows an optical image of a transferred BSCCO flake on the patterned substrate. Different optical contrast for suspended and collapsed micro-drums can be seen in the image. Fig. 1 (b) shows the topography of BSCCO flake alongside a height profile measured by AFM. Drums with an uneven topographic profile are not considered for measurements. The white dotted line indicates the location of the measured height profile. Transfer of flakes thinner than 16 nm (~ 5 UC)

^{a)}Electronic mail: v.singh@iisc.ac.in

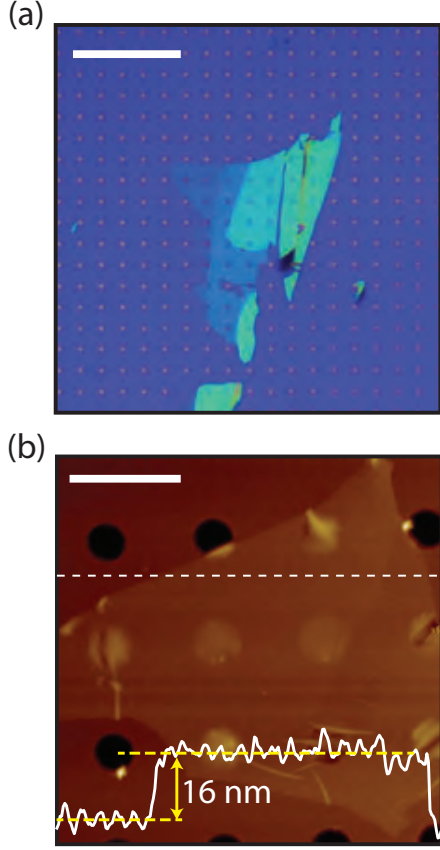


FIG. 1. (a) An optical microscope image of BSCCO flake on top of a patterned Si substrate coated with 285 nm of SiO₂. Difference in the contrast for suspended and collapsed drums can be seen. The scale-bar corresponds to 50 μm . (b) AFM image showing the topography of the flake. A height profile taken at the position marked by a dashed line is overlaid on the AFM image, showing a thickness of ~ 16 nm. The scale bar corresponds to 8 μm .

is a challenging task with our technique as they offer poor optical contrast, and their identification on PDMS remains difficult.

Elastic deformation by an AFM tip is a well-established method to characterize the elastic properties of nanoscale materials^{10,12,24}. An AFM cantilever with a known spring constant is used to apply a force on top of the suspended structure. This force deflects the flake depending on the elastic properties of the material and boundary conditions. In this study, we used an AFM tip with a spring constant of $k_{tip} = 5.6 \text{ N m}^{-1}$, measured using thermo-mechanical noise calibration²⁵. The spring constant of the tip relates the applied force F to the tip deflection Δz_{tip} , given by $F = k_{tip}\Delta z_{tip}$. The elastic deformation of the flake δ then can be expressed in terms of the net displacement of the AFM piezo Δz_p as: $\delta = \Delta z_p - \Delta z_{tip}$.

Fig. 2 (a) shows traces of loading-curve for flakes of different thicknesses while indenting at the center of the circularly-shaped suspended part. We do not observe any hysteresis be-

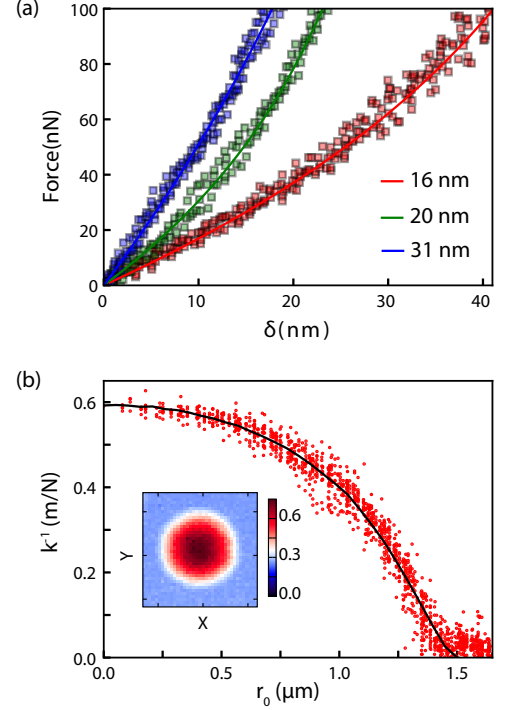


FIG. 2. (a) Force-displacement curves and corresponding fits for flakes with thicknesses of 16 nm (red), 20 nm (green), and 31 nm (blue). (b) Volumetric measurement of the compliance for a flake with a thickness of 16 nm. The solid line is fit to the data. The inset shows the complete compliance map measured from a flake of $\sim 3 \mu\text{m}$ diameter. Ticks on the inset figure are placed 1.5 μm apart.

tween loading and unloading curves, suggesting no slippage at the flake boundary. The loading curve is quite linear for the thick flake (31 nm). A nonlinear behavior can be easily observed for the thin flake (16 nm). Within continuum mechanics for an isotropic solid, the elastic deformation of the flake δ is related to the applied force F as:

$$F = \left[\frac{4\pi E}{3(1-\nu^2)} \left(\frac{t^3}{a^2} \right) \right] \delta + (\sigma\pi t) \delta + \left(\frac{q^3 E t}{a^2} \right) \delta^3, \quad (1)$$

where $q = 1/(1.049 - 0.15\nu - 0.16\nu^2)$ is a dimensionless constant, a and t are the radius and thickness of the suspended BSCCO flake, respectively²⁶. By using a Poisson's ratio of $\nu = 0.2$ for BSCCO¹⁹, and other geometrical quantities obtained from the AFM measurements, we fit the loading curves using Eq. 1, shown by the solid lines in Fig. 2 (a).

In the membrane-limit, the contribution from bending rigidity (first term in Eq. 1) can be neglected and the nonlinear relation between force and deformation can be used to extract the pre-stress and Young's modulus independently. In the plate-limit however, due to the comparable contributions from bending rigidity and tensile stress to the total elastic energy, it is impossible to separate out σ and E from the deformation measurement at the center of the flake alone. Therefore, we resort to the spatial measurement of local compliance, defined

as $k^{-1}(r_0, \theta_0) = (d\delta/dF)|_{r_0, \theta_0}$, over the suspended part of the flake²⁷. Spatial map of the measured local compliance over a grid of 64×64 points for a suspended flake of $\sim 3 \mu\text{m}$ diameter is shown in the inset of Fig. 2 (b). As the compliance profile is radially symmetric, Fig. 2 (b) shows the variation of k^{-1} with the distance from the center of the flake r_0 .

To extract the elastic properties of the BSCCO flakes from the spatial compliance maps, we perform finite element simulations using COMSOL (see Supplementary Material (SM) for details). For a linear elastic solid, the deformation under a point load can be well described by the Euler-Lagrange differential equation²⁸. However, when the contribution of bending rigidity and pre-stress to the elastic energy are comparable, it is difficult to find a closed-form solution of the elastic deformation $\delta(r, \theta)$ and hence compliance $k^{-1} = \partial\delta/\partial F$ ²⁴. To model the system, we consider the deformation of a linear elastic material under a load applied by an AFM tip of 40 nm radius. A rigid boundary condition is applied at the edge of the flake i.e. $\delta|_{r=a} = 0$. The sliding contact between the AFM tip and flake is captured by applying sliding contact boundary condition. Other material parameters such as the pre-stress and the Young's modulus are supplied as inputs to the model. Thus, the calculation of deflection under a small load applied at point r_0 away from the center of the flake allows calculating the local compliance.

Fig. 3(a) shows a contour plot of simulated compliance at the center ($r_0 = 0$) of a $3 \mu\text{m}$ diameter flake for different values of E , and σ . It is obvious from the plot that different combinations of (E, σ) can result in the same value of the compliance at the center of the flake. The radial shape of the compliance, however, depends on the ratio of pre-stress and bending rigidity $D = \frac{Et^3}{12(1-\nu^2)}$. Fig. 3 (b) shows the plots of the simulated radial profile of normalized compliance $k^{-1}/k^{-1}(r_0 = 0)$ for three different values of λ , defined as $\lambda = \sqrt{\frac{\sigma a^2}{D}}$. To fit the simulated results with the experimental data, we choose the contour of $k^{-1}(r_0 = 0)$ that matches with the AFM data. Along this contour, radial compliance profiles are computed for various combinations of (E, σ) to fit the experimentally obtained data. A result of this procedure is shown in Fig. 2 (b) by a black continuous line.

A plot summarizing the Young's modulus and the pre-stress for 7 different exfoliated flakes of varying thickness is shown in Fig. 3 (c, d). Detailed characterization of these flakes is provided in the SM. It is important to highlight that the pre-stress in these flakes results from the dry transfer process and is independent of material properties. Therefore, it spreads over significantly from 5 MPa to 46 MPa. However, the Young's modulus of rigidity is found to be in the range of 22 GPa to 30 GPa. Typically, elastic coefficients of ultra-thin samples, where the surface elastic energy is non-negligible to the bulk elastic energy, show a thickness-dependence^{12,14,29}. We do not observe any prominent thickness dependence in the Young's modulus of rigidity as the samples studied here are at least 16 nm thick.

The Young's modulus of rigidity can also be determined by a simple buckling technique²¹. We use this technique to independently verify the AFM results. A schematic representation of the steps used for buckling of BSCCO is shown in Fig. 4(a).

In this process, flake is transferred directly on a pre-stressed substrate. We use a PDMS substrate (PF-X4 6.5 mil from Gel-Pak), which has Young's modulus of $E_s = 492 \text{ kPa}$ and Poisson's ratio of $\nu = 0.5$ ³⁰. PDMS is elongated up to 30-40% of its original length in a direction perpendicular to its surface to generate the pre-stress. After releasing the stress from PDMS, BSCCO flake buckles with a particular wavelength.

Fig. 4 (b) shows an optical microscope image of buckled BSCCO flake over PDMS substrate. Different buckling wavelengths for different thickness are evidently visible. The wavelength of induced ripples (λ_b) is independent of initial stress and depends on the elastic properties of both flake and substrate, given by²¹:

$$\lambda_b = 2\pi t \left[\frac{(1-\nu_s^2)E}{3(1-\nu^2)E_s} \right]^{\frac{1}{3}}. \quad (2)$$

The wavelength is estimated by analyzing the optical microscope image of the buckled structure. For calibration of length, micron/pixel is calculated using a pre-patterned sample with known dimensions. The thickness of the flake was measured to be 7 UC using AFM. The average value of λ_b is $\sim 2.11 \mu\text{m}$, calculated from four different data points. Using Eq. 2, we estimated the Young's modulus of rigidity to be 24.5 GPa, which is similar to values obtained from the AFM measurement.

It is interesting to contrast our results on few UC samples to the observations made on the bulk crystals of BSCCO and other high- T_c layered superconductors. The Young's modulus of rigidity for bulk crystals of BSCCO has been reported over a range of values (see Table I). Crystalline quality dependent variations in the Young's modulus of rigidity has been observed for other layered high- T_c superconductors such as $\text{YBa}_2\text{Cu}_3\text{O}_7$ ^{19,31}. The reduction in modulus of rigidity and breaking strength can be attributed to defects formed during the crystal growth process^{14,32}. Under a normal applied load, the material tends to yield at the defect sites first, before stretching of the atomic bonds³³. Importance of the defect density in determining elastic coefficients and the breaking strength has been reported for mesoscopic samples of different materials^{14,34,35}. Layered superconductors having several weakly interacting layers with defects are therefore expected to show reduced material stiffness.

For application towards the composite nanoelectromechanical devices, the resonant frequency of the mechanical resonator is an important design parameter. From the variation in the Young's modulus and pre-stress reported in this study, we expect the mechanical resonance frequency to be in the range of 6 MHz to 18 MHz for 5 UC thick crystals of $6 \mu\text{m}$ diameter, as also observed experimentally⁶. We further note that for few UC thick mechanical resonators, the resonant frequency is primarily dominated by the pre-stress induced by the exfoliation process. The expected high frequency of BSCCO mechanical resonators and typical linewidths of superconducting microwave resonators ($< 500 \text{ kHz}$) place these devices in the sideband-resolved limit, an important criterion for experiments in the quantum limit³⁶.

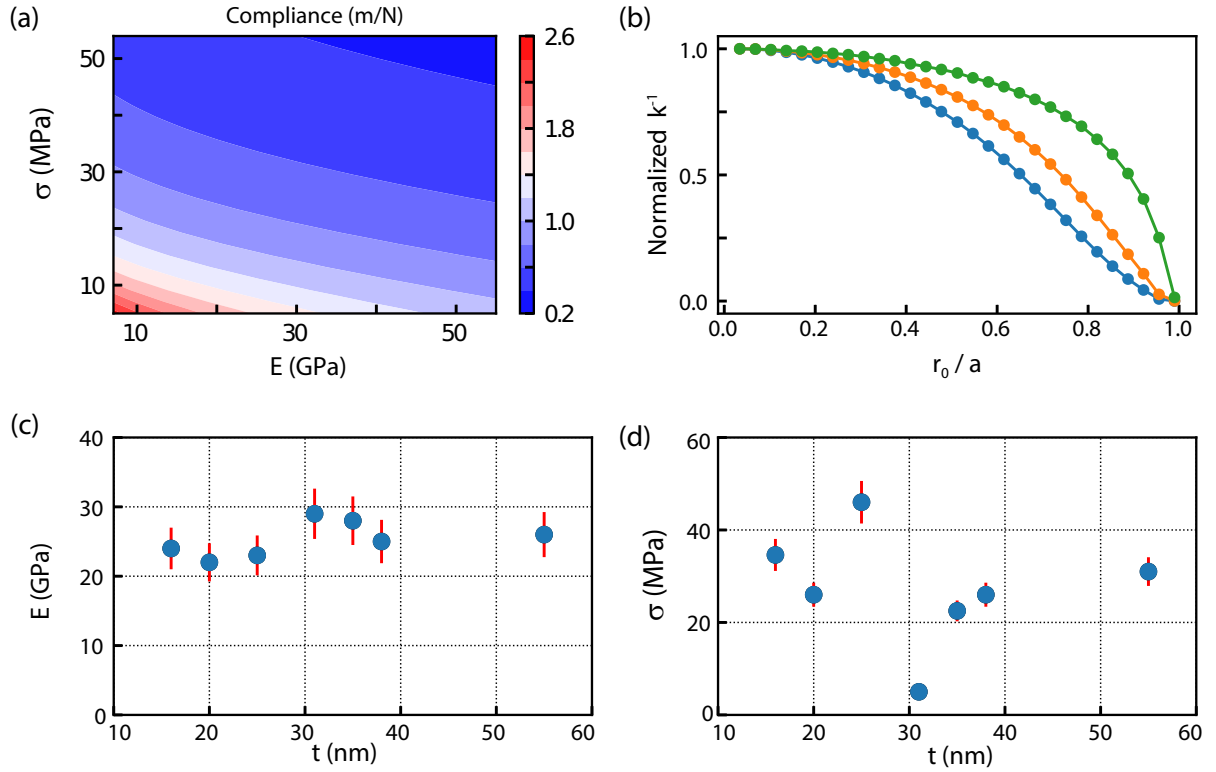


FIG. 3. (a) Contour plot showing local compliance k^{-1} at the center of the drum with a variation of the Young's modulus and pre-stress, simulated by finite element method. (b) The simulated radial profile of compliance for different values of λ given by 1 (blue), 10 (orange) and 100 (green), respectively. Panels (c) and (d) show the extracted value of the Young's modulus and pre-stress of BSCCO flakes of different thicknesses. The error bars are calculated from the spread in the radial compliance data.

TABLE I. Summary of Young's modulus of rigidity for high- T_c superconductors

Material	Structure	Technique	E[GPa]
BSCCO	bulk polycrystalline	ultrasonic velocity ¹⁹	38.8
	bulk single crystal	vibrating reed ²⁰	70
	few unit cells thick	AFM and buckling methods [This work]	22 - 30
YBa ₂ Cu ₃ O ₇	bulk single crystal	ultrasonic velocity ³¹	46.4

To summarize, we have studied the mechanical properties of exfoliated thin BSCCO crystals using deformation caused by an AFM tip. Finite element simulations are used for the numerical analysis of spatial compliance maps, and to extract the Young's modulus and pre-stress. The reported mechanical properties could potentially be useful in engineering nano-electromechanical resonators of BSCCO for various applications.

SUPPLEMENTARY MATERIAL

See supplementary material for the characterization of additional flakes and details of simulations.

ACKNOWLEDGMENTS

This work was supported by STC-ISRO. VS acknowledges the fabrication facilities at CeNSE and AFM facilities at the Department of Physics, IISc-Bangalore, funded by the Department of Science and Technology. MMD acknowledges Nanomission grant SR/NM/NS-45/2016 and the Department of Atomic Energy for support.

¹Akinwande, D., Petrone, N., and Hone, J. *Nature Communications* **5**, 5678 (December (2014)).

²Castellanos-Gomez, A., Singh, V., van der Zant, H. S. J., and Steele, G. A. *Annalen der Physik* **527**(1-2), 27–44 (January (2015)).

³Singh, V., Bosman, S. J., Schneider, B. H., Blanter, Y. M., Castellanos-Gomez, A., and Steele, G. A. *Nature Nanotechnology* **9**(10), 820–824 (October (2014)).

⁴Güttinger, J., Noury, A., Vergara-Cruz, J., and Bachtold, A. *Nature Communications* **7**, ncomms12496 (August (2016)).

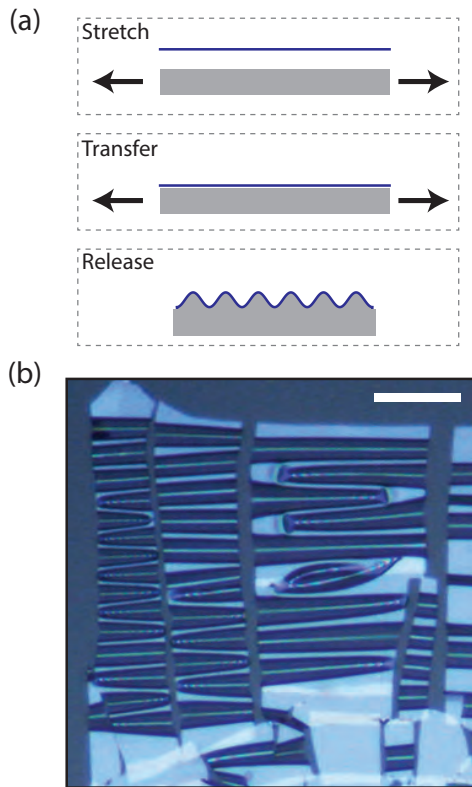


FIG. 4. (a) A schematic representation of the steps used to obtain buckled flake on top of PDMS. (b) An optical microscope image of buckled BSCCO flake. The scale bar corresponds to 12 μm .

- ⁵Will, M., Hamer, M., Müller, M., Noury, A., Weber, P., Bachtold, A., Gorbachev, R. V., Stampfer, C., and Güttinger, J. *Nano Letters* **17**(10), 5950–5955 October (2017).
- ⁶Sahu, S. K., Vaidya, J., Schmidt, F., Jangade, D., Thamizhavel, A., Steele, G., Deshmukh, M. M., and Singh, V. *2D Materials* **6**(2), 025027 February (2019).
- ⁷Singh, V., Shevchuk, O., Blanter, Y. M., and Steele, G. A. *Physical Review B* **93**(24), 245407 June (2016).
- ⁸Davidovikj, D., Alijani, F., Cartamil-Bueno, S. J., Zant, H. S. J. v. d., Amabili, M., and Steeneken, P. G. *Nature Communications* **8**(1), 1253 November (2017).
- ⁹Binek, C. *Scientific Reports* **7**(1), 4906 July (2017).
- ¹⁰Poot, M. and van der Zant, H. S. J. *Applied Physics Letters* **92**(6), 063111 February (2008).
- ¹¹Sengupta, S., Solanki, H., Singh, V., Dhara, S., and Deshmukh, M. *Physical Review B* **82**(15), 155432 October (2010).
- ¹²Lee, C., Wei, X., Kysar, J. W., and Hone, J. *Science* **321**(5887), 385–388 July (2008).
- ¹³Castellanos-Gomez, A., Poot, M., Steele, G. A., van der Zant, H. S. J., Agrait, N., and Rubio-Bollinger, G. *Advanced Materials* **24**(6), 772–775 February (2012).
- ¹⁴Falin, A., Cai, Q., Santos, E. J. G., Scullion, D., Qian, D., Zhang, R., Yang, Z., Huang, S., Watanabe, K., Taniguchi, T., Barnett, M. R., Chen, Y., Ruoff, R. S., and Li, L. H. *Nature Communications* **8**, 15815 June (2017).
- ¹⁵Liu, K., Yan, Q., Chen, M., Fan, W., Sun, Y., Suh, J., Fu, D., Lee, S., Zhou, J., Tongay, S., Ji, J., Neaton, J. B., and Wu, J. *Nano Letters* **14**(9), 5097–5103 September (2014).
- ¹⁶Huang, Y., Sutter, E., Shi, N. N., Zheng, J., Yang, T., Englund, D., Gao, H.-J., and Sutter, P. *ACS Nano* **9**(11), 10612–10620 November (2015).
- ¹⁷Sterpetti, E., Biscaras, J., Erb, A., and Shukla, A. *Nature Communications* **8**(1), 2060 December (2017).
- ¹⁸Liao, M., Zhu, Y., Zhang, J., Zhong, R., Schneeloch, J., Gu, G., Jiang, K., Zhang, D., Ma, X., and Xue, Q.-K. *Nano Letters* **18**(9), 5660–5665 September (2018).
- ¹⁹Sihan, L., Yusheng, H., Chongde, W., and Zhaohui, S. *Superconductor Science and Technology* **2**(2), 145–148 August (1989).
- ²⁰Nes, O.-M., Castro, M., Slaski, M., Laegreid, T., Fossheim, K., Motohira, N., and Kitazawa, K. *Superconductor Science and Technology* **4**(1S), S388–S390 January (1991).
- ²¹Stafford, C. M., Harrison, C., Beers, K. L., Karim, A., Amis, E. J., Van-Landingham, M. R., Kim, H.-C., Volksen, W., Miller, R. D., and Simonyi, E. E. *Nature Materials* **3**(8), 545 August (2004).
- ²²Jindal, A., Jangade, D. A., Kumar, N., Vaidya, J., Das, I., Bapat, R., Parmar, J., Chalke, B. A., Thamizhavel, A., and Deshmukh, M. M. *Scientific Reports* **7**(1) December (2017).
- ²³Castellanos-Gomez, A., Buscema, M., Molenaar, R., Singh, V., Janssen, L., van der Zant, H. S. J., and Steele, G. A. *2D Materials* **1**(1), 011002 April (2014).
- ²⁴Norouzi, D., Müller, M. M., and Deserno, M. *Physical Review E* **74**(6), 061914 December (2006).
- ²⁵Sader, J. E., Chon, J. W. M., and Mulvaney, P. *Review of Scientific Instruments* **70**(10), 3967–3969 September (1999).
- ²⁶Timoshenko, S. and Woinowsky-Krieger, S. *Theory of plates and shells*. McGraw-Hill, (1959).
- ²⁷Radmacher, M., Fritz, M., Cleveland, J. P., Walters, D. A., and Hansma, P. K. *Langmuir* **10**(10), 3809–3814 October (1994).
- ²⁸Landau, L. D., Pitaevskii, L. P., Kosevich, A. M., and Lifshitz, E. M. *Theory of elasticity*. Pergamon Press, (1986).
- ²⁹Miller, R. E. and Shenoy, V. B. *Nanotechnology* **11**(3), 139–147 July (2000).
- ³⁰Iguiniz, N., Frisenda, R., Bratschitsch, R., and Castellanos-Gomez, A. *Advanced Materials* **0**(0), 1807150.
- ³¹Bishop, D. J., Ramirez, A. P., Gammel, P. L., Batlogg, B., Rietman, E. A., Cava, R. J., and Millis, A. J. *Physical Review B* **36**(4), 2408 (1987).
- ³²Song, L., Ci, L., Lu, H., Sorokin, P. B., Jin, C., Ni, J., Kvashnin, A. G., Kvashnin, D. G., Lou, J., Yakobson, B. I., and Ajayan, P. M. *Nano Letters* **10**(8), 3209–3215 August (2010).
- ³³Griffiths, A. A. *Philos. Trans. R. Soc. London Ser. A* **221**, 163 January (1921).
- ³⁴Zandiatashbar, A., Lee, G.-H., An, S. J., Lee, S., Mathew, N., Terrones, M., Hayashi, T., Picu, C. R., Hone, J., and Koratkar, N. *Nature Communications* **5**, 3186 January (2014).
- ³⁵Lopez-Polin, G., Gomez-Navarro, C., Parente, V., Guinea, F., Katsnelson, M. I., Perez-Murano, F., and Gomez-Herrero, J. *Nature Physics* **11**(1), 26–31 January (2015).
- ³⁶Poot, M. and van der Zant, H. S. J. *Physics Reports* **511**(5), 273–335 February (2012).